Optical Analysis of Perovskite/Silicon Tandem Solar Cells
Supporting Information

Yajie Jiang[1], Ibraheem Almansouri[2], Shujuan Huang[1], Trevor Young[1], Yang Li[1], Yong Peng[3], Qicheng Hou[3], Leone Spiccia[4], UdoBach[3], Yi-BingCheng[3], Martin A. Green[1], Anita Ho-Baillie[1]*

1: Australian Centre for Advanced Photovoltaics, University of New South Wales, Sydney 2052, Australia

2: Institute Center for Energy (iEnergy), Department of Electrical Engineering and Computer Science, Masdar Institute, Abu Dhabi, UAE

3: Department of Materials Science and Engineering, Monash University, Victoria 3800, Australia

4: School of Chemistry, Monash University, Victoria 3800 Australia

Materials

Methylamine (CH_3NH_2, 33% in ethanol), hydroiodic acid (HI, 57% in water), lead iodide (PbI_2, 99.999%), 4-tert-butylpyridine (TBP, 97%), lithium bis(trifluoromethylsulphonyl)imide (LiTFSi, 99.95%), N,N-dimethylformamide (DMF, 99.8%), chlorobenzene (99.8%), acetonitrile (99.8%) and molybdenum trioxide (MoO_3, 99.5%) have been purchased from Sigma Aldrich. Gold was purchased from A&E Metals. 2,2',7,7'-tetrakis(N,N-di-p-methoxyphenylamine)-9,9-spirobi- fluorene (spiro-OMeTAD, 99.5%) was from Luminescence Technology Corp. Methylammonium iodide (CH_3NH_3I) was synthesized by Dr. Steffen Myer by reacting CH_3NH_2 with HI and then purified via recrystallization.

Sample Fabrication

Detailed sample preparation methods have been published elsewhere [1]. Generally, the dense TiO_2 hole-blocking layer on FTO glass (TEC-8 manufactured by NEG with sheet

resistivity of 9 Ω/❑) was made by spray pyrolysis of a bis(isopropoxide)-bis (acetylacetonate)titanium(IV) solution at 450°C. Substrates were annealed at 450°C for 10 mins to crystalize the TiO_2 layer. Perovskite (45 wt% $CH_3NH_3PbI_3$ DMF solution, prepared from PbI_2 and CH_3NH_3 in a molar ratio of 1:1) and spiro-OMeTAD (prepared by dissolving 41.6 mg spiro-OMeTAD in 0.5 mL chlorobenzene, adding 7.5 μL of a stock solution of 520 mg mL^{-1} lithium bis(trifluoromethylsulphonyl)imide in acetonitrile and 16.9 μL of 4-tert-butylpyridine) layers were fabricated by spin coating of solutions (30 s of 6500 rpm and 30 s of 3000 rpm were applied respectively). Importantly, the perovskite layer was spin coated with gas assistance to improve the microstructure of the perovskite layer. The details of gas-assisted method can be found in the reference [2]. 100°C for 10 mins was used to form perovskite crystals after perovskite solution was spin coated. Samples were cooled down for 5 mins before the subsequent Spiro spin-coating. Finally the devices were completed by thermally evaporating (utilizing Edwards Thermal Evaporator) MoO_3/gold/MoO_3 semitransparent electrode under vacuum (~$3x10^{-6}$ Torr). The deposition rate was set to be 0.1 nm/s for MoO_3 and 0.05 nm/s for gold.

Optical Measurement and Modelling

Optical modelling of the semi-transparent perovskite cell requires knowledge of the optical properties (refractive index $n(\lambda)$ and extinction coefficient $k(\lambda)$) of each layer in the cell. Reflection, transmission and spectroscopic ellipsometry measurements were carried out on the complete structure and on each layer individually. WVASE® was used to model the optical properties and layer thicknesses of the samples based on the reflection and transmission data [3]. The optical constants of the individual layers were used to establish an optical model of the complete planar semi-transparent perovskite solar cell, to ascertain the optical losses of such a cell when implemented in a perovskite on silicon tandem structure.

FTO Glass

Reflectance (R) and transmittance (T) of the TEC-8 glass were measured using a Varian Cary UV-VIS-NIR spectrophotometer at close to normal incidence using a light spot about 5 mm in diameter. WVASE® was used to model the optical properties and layer thicknesses of the TEC-8 glass, based on the reflection and transmission data [3].

TEC-8 glass consists of a soda-lime glass substrate, thin undoped SnO_2, thin SiO_2 and a thick layer of fluorine doped tin-oxide (SnO_2:F), in order. Literature values were taken for the optical constants of the soda-lime glass, SnO_2 and SiO_2 [4].

The experimental and modelled reflection *R* and transmission *T* of TEC-8 glass are shown in Figure S1(a) and (b) respectively. The wavelength-dependent optical constants of the SnO_2:F film determined by fitting *R* and *T* are shown in Figure S1 (c). The thicknesses of SnO_2, SiO_2, and SnO_2:F layers were determined as 34 nm, 29 nm, and 548 nm, respectively. A rough surface layer was determined with a thickness of 31 nm and 47 % void based on the effective medium approximation using Bruggeman's model [5]. The roughness of the TEC-8 glass surface resulted in an unexpected scattering of the normal incidence reflection and transmission (Figure S1(b)). Surface roughness of the SnO_2:F film also makes accurate optical modelling more difficult, leading to the discrepancies observed in Figure S1.

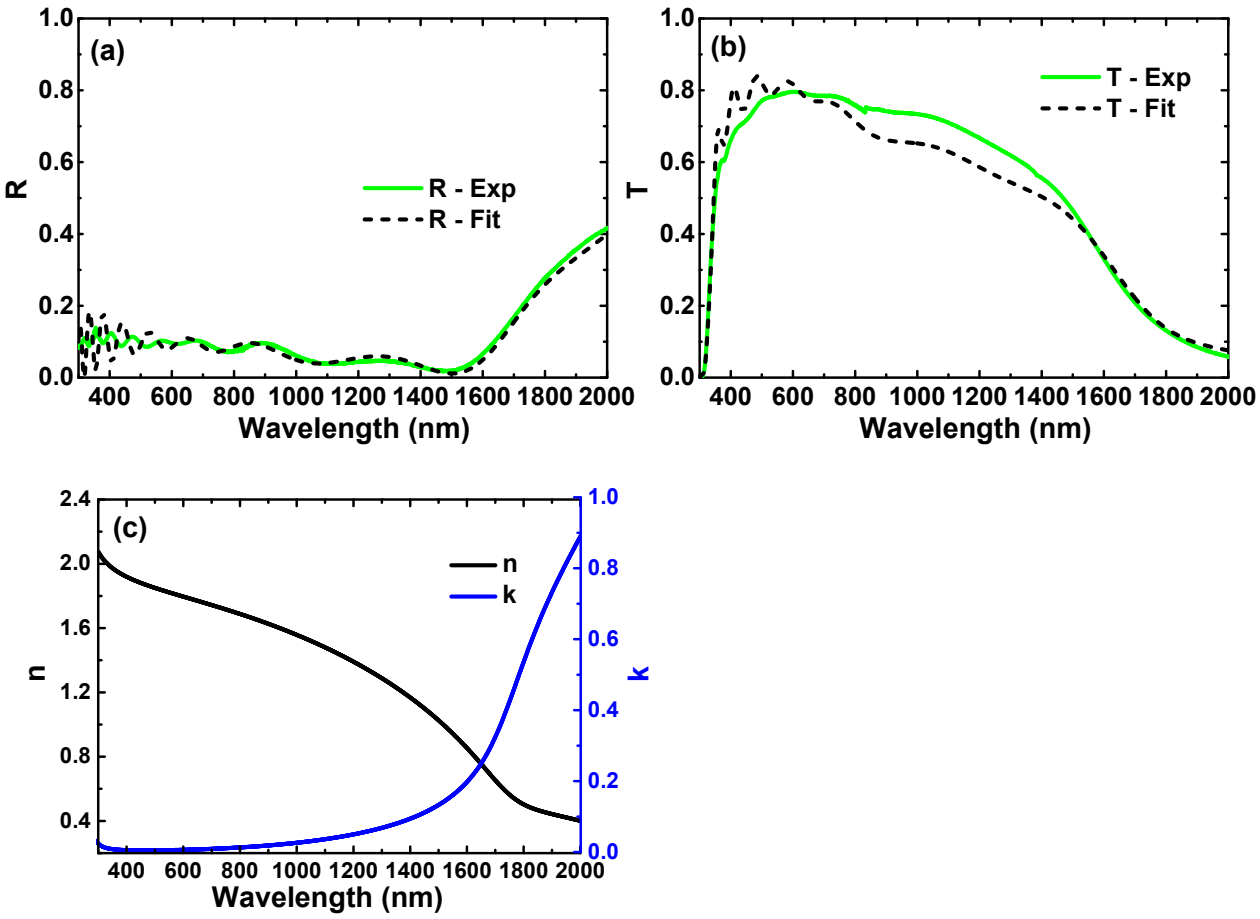

Figure S1 Modelled (black dashed lines) and experimental (green solid lines) (a) reflection R and (b) transmission T; and (c) refractive index n and extinction coefficient k of TEC-8 glass substrate.

Because it is difficult to build up an accurate optical model for thin films on rough substrates like TEC-8 glass, modeling of optical properties of each layer in the stack was performed on individual layers deposited on flat glass substrates.

Ellipsometry and transmission data were analyzed using WVASE® to determine the optical properties of the film/flat glass samples. Reflection data were not required because the ellipsometry was carried out in reflection mode. Transmission data provide complementary information due to the different path length the light travels in the sample. All ellipsometry data in this study were collected from three angles of incidence; 65°, 70° and 75°, except for the spiro-OMeTAD/flat glass sample where incident angles of 45°, 50° and 55° were used. Larger angles of incidence lead to a larger spot size on the sample and this introduces more uncertainty in the measured data when there is thickness non-uniformity, such as was the case for the spin-coated spiro-OMeTAD film. Subsequently, the optical properties of each individual layer were used to calculate the electric field distribution inside the complete tandem device stack via the transfer matrix method [6, 7]. The interference of coherent reflected and transmitted waves at each interface, as well as the optical absorption distribution in each layer could be determined.

Thin Glass Substrate

A Cauchy oscillator and two Gaussian dispersions were used to model the absorption of the 1 mm thick flat glass substrate. Figure S2(a), (b) and (c) show the experimental and modelled amplitude component Ψ, phase difference Δ and transmission T of a thin flat glass substrate respectively. The combination of these three was used to determine the refractive index n and extinction coefficient k shown in Figure S2(d). The experimental and simulated data agree well.

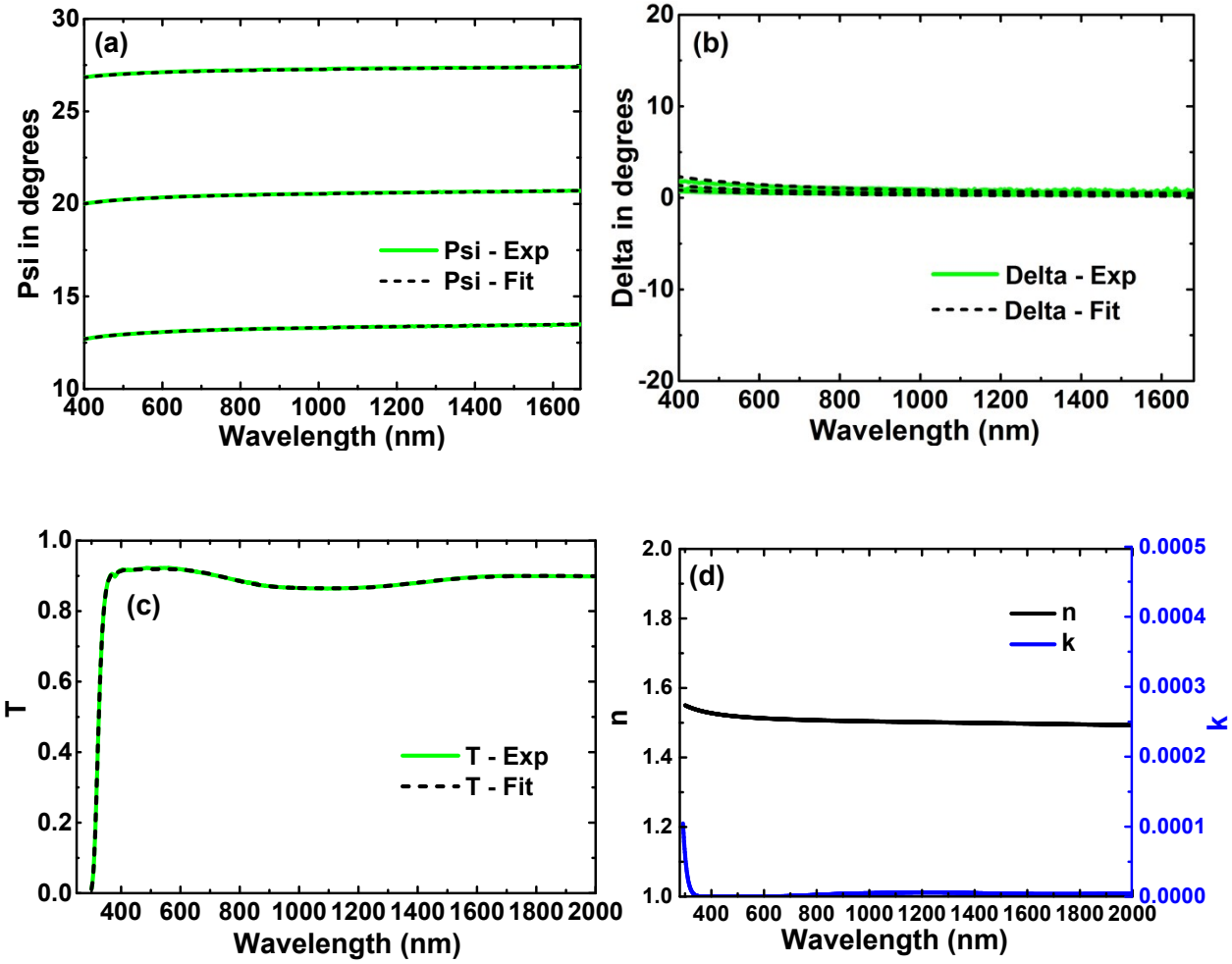

Figure S2 Modelled (black dashed lines) and experimental (green solid lines) (a) amplitude component Ψ; (b) phase difference Δ; (c) transmission T and (d) refractive index n and extinction coefficient k of a thin flat glass substrate. The ellipsometry data are collected from three incident angles; 65°, 70° and 75°.

TiO_2 compact layer on glass

A Tauc-Lorentz dispersion was used to model the TiO_2 thin film on borosilicate glass by combining a Tauc band-edge with Lorentz broadening function [41]. Figure S3(a-c) show the experimental and modelled Ψ, Δ, and T of the TiO_2 film, respectively. These results were used to determine the refractive index n and extinction coefficient k of compact TiO_2 layer shown in Figure S3(d). The TiO_2 film thickness was determined to be 44 nm.

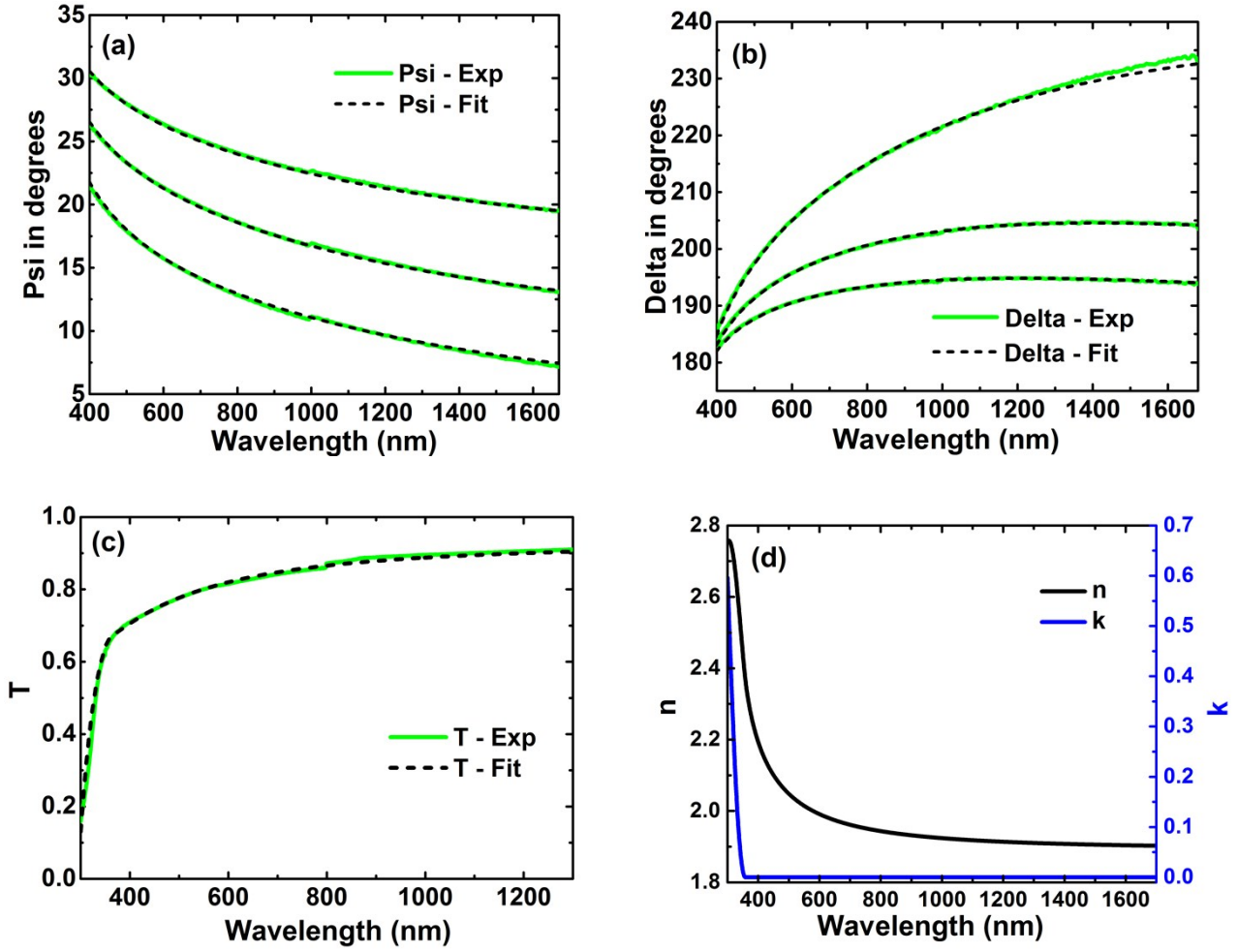

Figure S3 Modelled (red dash lines) and experimental (red solid lines) (a) amplitude component Ψ; (b) phase difference Δ; (c) Transmission T; and (d) refractive index n and extinction coefficient k of TiO_2 thin film on borosilicate glass substrate.

Spiro-OMeTAD

A spin-coated film of spiro-OMeTAD deposited on a glass substrate was modelled similarly. A Cauchy model and an extra Gaussian dispersion were used to account for the short wavelength absorption feature. Residual discrepancy in the ultra violet may be due to the poor coverage of spiro-OMeTAD on this substrate. The detailed fitting plots and optical constants are shown in Figure S4. The spiro-OMeTAD film was found to be 273 nm thick. Large k values determined in the ultra-violet region indicate strong absorption in the spiro-

OMeTAD layer, which will introduce parasitic losses when illuminating from the transparent contact side.

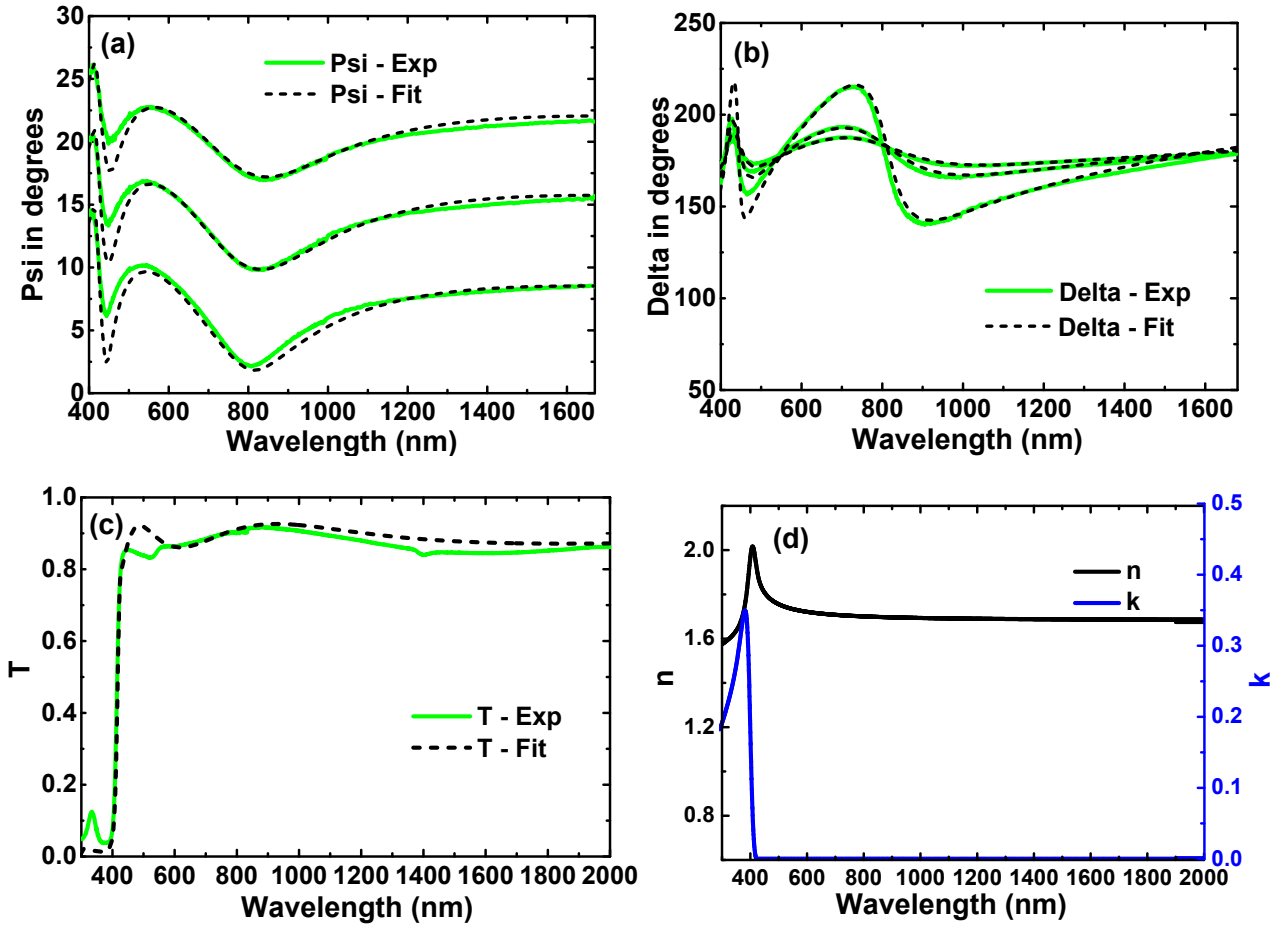

Figure S4 Modelled (black dashed lines) and experimental (green solid lines) (a) amplitude component Ψ; (b) phase difference Δ; (c) transmission T and (d) refractive index n and extinction coefficient k of spiro-OMeTAD on a flat glass substrate. The ellipsometry data are collected from three incident angles; 45°, 50° and 55°.

Transparent Electrode

The transparent electrode of the semi-transparent perovskite solar cell shown in Figure 2 is composed of a MoO_3/Au/MoO_3 stack. The molybdenum trioxide layer underneath the gold film serves as a good nucleation surface allowing the growth of a thin, uniform and continuous metal film.

The optical properties of the top MoO_3 and Au layers were characterized individually using the same approach as that described above for perovskite and spiro-OMeTAD layers. The bottom 5 nm thin MoO_3 layer was evaporated using exactly same process with the top MoO_3 layer so these two layers were assumed to have the same optical properties. The fitted data and optical constants are shown in Figure S5 and Figure S6. Thicknesses of 42 nm and 9 nm for the dielectric layer and conducting metal layer were obtained, respectively.

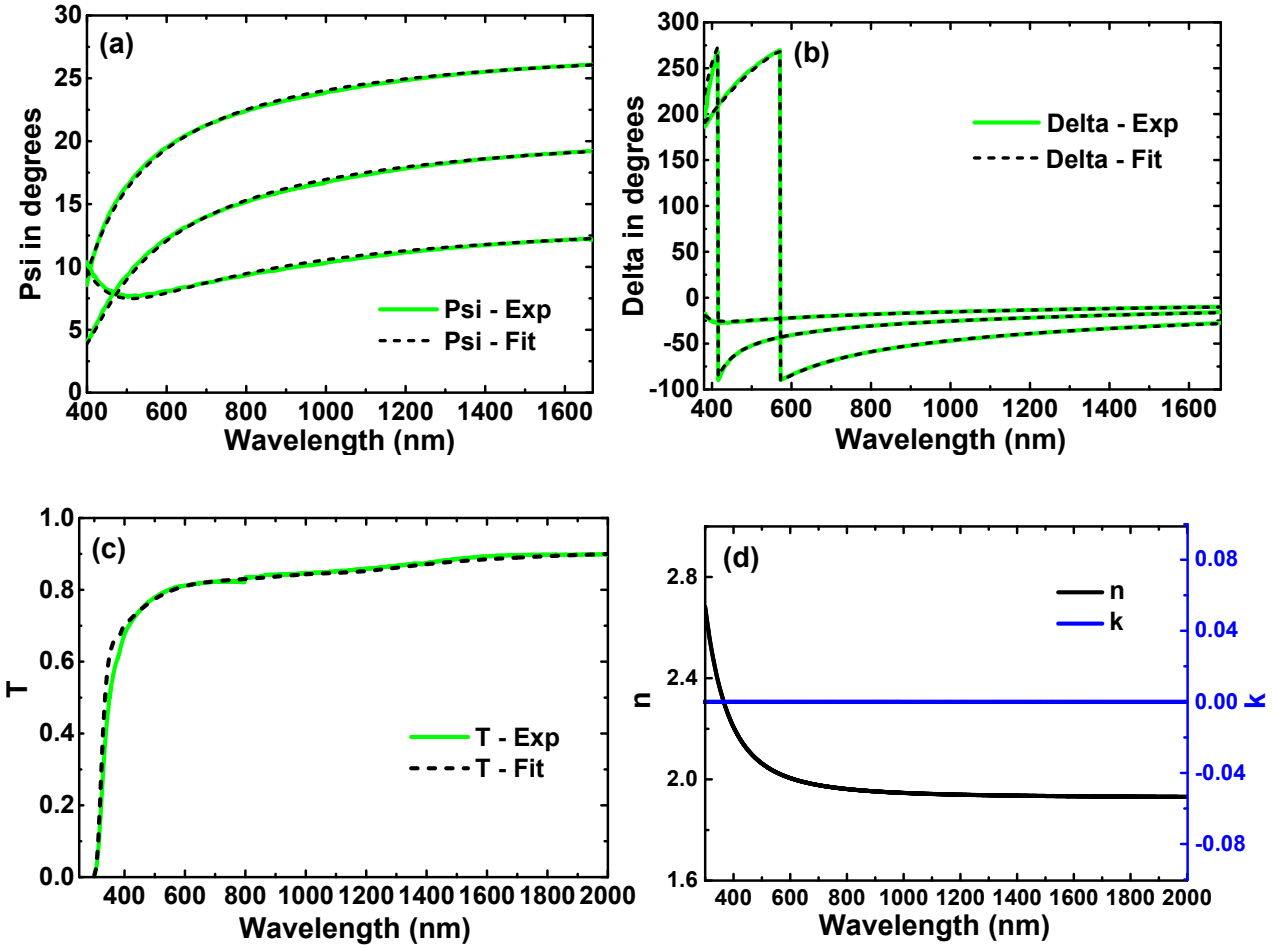

Figure S5 Modelled (black dashed lines) and experimental (green solid lines) (a) amplitude component Ψ; (b) phase difference Δ; (c) transmission T and (d) refractive index n and extinction coefficient k of a MoO_3 thin film on a flat glass substrate. The ellipsometry data are collected from three incident angles; 65°, 70° and 75°.

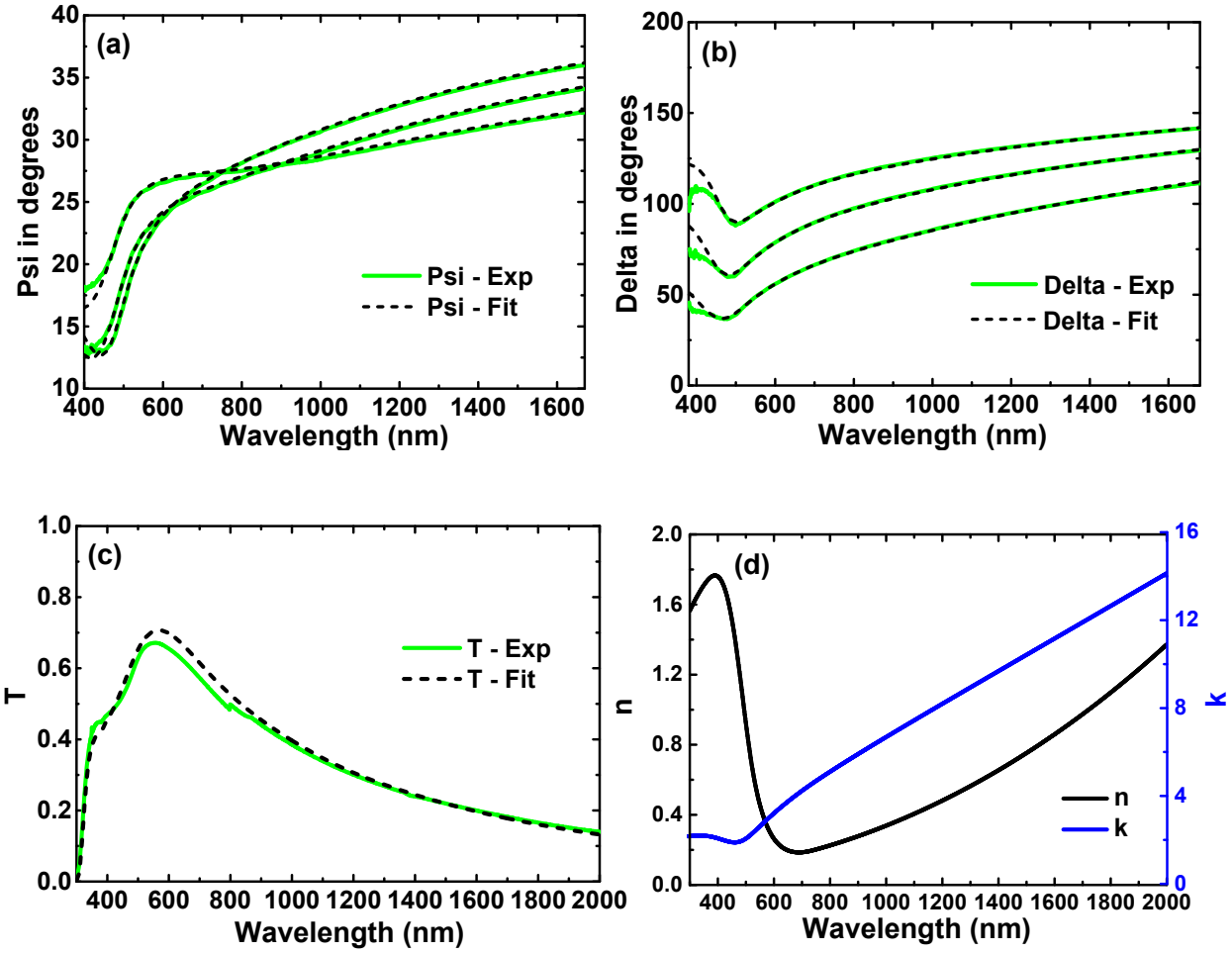

Figure S6 Modelled (black dashed lines) and experimental (green solid lines) (a) amplitude component Ψ; (b) phase difference Δ; (c) transmission T and (d) refractive index n and extinction coefficient k of a gold film on a flat glass substrate. The ellipsometry data are collected from three incident angles; 65°, 70° and 75°.

Performance of Solar Cell Devices

The efficiencies of the photovoltaic devices were calculated using the principle of detailed balance according to Shockley-Queisser theory [8]. In thermal equilibrium, the photon flux density (N in units of W/m^2) emitted by a solar cell behaving as a blackbody source with a temperature T, is approximated using Planck's blackbody radiation law [9], which is given by;

$$N(E,T) = \frac{2\pi n_r^2}{\mathrm{h}^3 c^2} \int_0^{\infty} \frac{a(E)E^2}{exp\left(\frac{E}{kT}\right) - 1} dE \quad \text{(S1)}$$

where n_r is the refractive index of the surrounding medium i.e. n_r =1 for air, h is Planck's constant (6.626x10^{-34} Js), c is the speed of light in vacuum (2.998x10^8 m/s), $a(E)$ is the material's absorbance, E is the photon energy, and k is Boltzmann's constant (1.3807 x 10^{-23} J/K).

Under illumination from an illumination source such as the sun, the photon flux density absorbed by the solar cell device results in photo-generated current within the device which is given by;

$$N_s(E) = \int_0^{\infty} a(E) N_{AM1.5G}(E) dE \quad \text{(S2)}$$

where $N_{AM1.5G}(E)$ is the photon flux of the incident solar spectrum i.e. ASTM G173-03 AM1.5G [10]. Therefore, under the detailed balance approach, the difference between the absorbed photons in the device and the emitted photons from the device gives the electrical output current. Thereby, the current density J(V) flowing through the solar cell device is mathematically described under an applied bias voltage V by;

$$J(V) = \int_0^{\infty} a(E) N_{AM1.5G}(E) dE - e^{\frac{qV}{kT}} \frac{2\pi n_r^2}{\mathrm{h}^3 c^2} \int_0^{\infty} \frac{a(E)E^2}{exp\left(\frac{E}{kT}\right) - 1} dE \quad \text{(S3)}$$

The power produced by the solar cell devices (S4-a) and thus the conversion efficiency (S4-b) are given by;

$$P = VJ \quad \text{(S4-a)}$$

$$\eta = P_{MPP}/P_{IN} \quad \text{(S4-b)}$$

where P_{MPP} is the maximum power point and P_{IN} is the incident solar power.

The conversion efficiency of multi-junction devices depends upon the interconnection configuration. In an unconstrained multi-junction structure with N terminals where N is twice the number of junctions r, each device operates independently at its own maximum power point, as given by S5-a. Conversely, a two-terminal configuration requires that the photo-

generated current is limited by the junction with the lowest current, as represented by S5-b. In the case that all junctions are current matched, the tandem efficiency is approximately equal to the sum of the individual cell efficiencies.

$$P_{Tandem} = \sum_{i=1}^{r} I_i V_i \quad \text{(S5-a)}$$

$$P_{Tandem} = I \sum_{i=1}^{r} V_i \quad \text{(S5-b)}$$

References

1. E. Della Gaspera, Y. Peng, Q. Hou, L. Spiccia, U. Bach, J. J. Jasieniak, Y.-B. Cheng, *Ultra-thin high efficiency semitransparent perovskite solar cells.* Nano Energy, 2015. **13**(0): p. 249-257.
2. F. Huang, Y. Dkhissi, W. Huang, M. Xiao, I. Benesperi, S. Rubanov, Y. Zhu, X. Lin, L. Jiang, Y. Zhou, A. Gray-Weale, J. Etheridge, C. R. McNeill, R. A. Caruso, U. Bach, L. Spiccia, Y.-B. Cheng, *Gas-assisted preparation of lead iodide perovskite films consisting of a monolayer of single crystalline grains for high efficiency planar solar cells.* Nano Energy, 2014. **10**: p. 10-18.
3. *Guide to using WVASE® 32*. J. A. Woollam Co., Inc.
4. J. Chen, *Spectroscopic ellipsometry studies of II-VI semiconductor materials and solar cells*. 2010, The University of Toledo.
5. D. A. G. Bruggeman, *Berechnung verschiedener physikalischer Konstanten von heterogenen Substanzen. I. Dielektrizitätskonstanten und Leitfähigkeiten der Mischkörper aus isotropen Substanzen.* Annalen Der Physik, 1935. **416**(7): p. 636-664.
6. O. S. Heavens, *Optical Properties of Thin Solid Films*. 1991: Dover Publications.
7. G. F. Burkhard, E. T. Hoke, M. D. McGehee, *Accounting for Interference, Scattering, and Electrode Absorption to Make Accurate Internal Quantum Efficiency Measurements in Organic and Other Thin Solar Cells.* Advanced Materials, 2010. **22**(30): p. 3293-3297.
8. W. Shockley, H. J. Queisser, *Detailed Balance Limit of Efficiency of p‐n Junction Solar Cells.* Journal of Applied Physics, 1961. **32**(3): p. 510-519.
9. M. Planck, *On the Law of Distribution of Energy in the Normal Spectrum.* Annalen Der Physik, 1901. **309**(3): p. 553-563.
10. S. Colella, E. Mosconi, P. Fedeli, A. Listorti, F. Gazza, F. Orlandi, P. Ferro, T. Besagni, A. Rizzo, G. Calestani, G. Gigli, F. De Angelis, R. Mosca, *MAPbI3-xClx*

Mixed Halide Perovskite for Hybrid Solar Cells: The Role of Chloride as Dopant on the Transport and Structural Properties. Chemistry of Materials, 2013. **25**(22): p. 4613-4618.